# Comparison of Single Crystal and Polycrystalline $LiNi_{0.5}Mn_{0.3}Co_{0.2}O_2$ Positive Electrode Materials for High Voltage Li-Ion Cells

**Jing Li,[a] Andrew R. Cameron,[b] Hongyang Li,[a] Stephen Glazier,[a] Deijun Xiong,[c] M. Chatzidakis,[d] Jenn Allen,[c] G. A. Botton,[d] and J. R. Dahn[a,c,*,z]**

[a]*Physics and Atmosphere Science, Dalhousie University, Halifax, NS B3H 3J5, Canada*
[b]*Department of Physics, University of Prince Edward Island, Charlottetown, PE C1A 4P3, Canada*
[c]*Department of Chemistry, Dalhousie University, Halifax, NS B3H 3J5, Canada*
[d]*Materials Science and Engineering, Canadian Centre for Electron Microscopy, McMaster University, Hamilton, Ontario L8S 4L7, Canada*

Single-crystal $LiNi_{0.5}Mn_{0.3}Co_{0.2}O_2$ (NMC532) with a grain size of 2–3 μm was compared to conventional polycrystalline uncoated NMC532 and polycrystalline $Al_2O_3$-coated materials in this work. Studies were made to determine how single crystal NMC532 material with large grain size could be synthesized. Ultra high precision coulometry (UHPC), in-situ gas measurements and isothermal microcalorimetry were used to make comparative studies of the three materials in Li-ion pouch cells. All the diagnostic measurements suggested that the single crystal material should yield Li-ion cells with longer lifetime. Long-term cycling tests verified these predictions and showed that cells with single crystal NMC532 exhibited much better capacity retention than cells with the polycrystalline materials at both 40°C and 55°C when tested to an upper cutoff potential of 4.4 V. The reasons for the superior performance of the single crystal cells were explored using thermogravimetric analysis/mass spectrometry experiments on the charged electrode materials. The single crystal materials were extremely resistant to oxygen loss below 100°C compared to the polycrystalline materials. The major drawback of the single crystal material is its slightly lower specific capacity compared to the polycrystalline materials. However, this may not be an issue for Li-ion cells designed for long lifetime applications.


Manuscript submitted March 17, 2017; revised manuscript received May 8, 2017. Published May 23, 2017.

Lithium ion batteries with high energy density, long lifetime and low cost need to be developed for applications in electric vehicles and stationary energy storage. The family of $Li(Ni_xMn_yCo_z)O_2$ ($x + y + z = 1$) (NMC) materials with high nickel and low cobalt are used as positive electrode materials in lithium ion cells.[1,2] One simple way to increase the energy density of NMC lithium ion cells is to increase their upper cutoff voltage which gives access to higher specific capacity from the positive electrode.[3,4] However, increasing the upper cutoff voltage usually decreases the lifetime of cells due to an acceleration of 'unwanted' parasitic reactions between the electrolyte and the delithiated positive electrode surface at high voltages. Such reactions include oxidation of species found in the electrolyte, transition metal dissolution, etc.[5–7] In addition, structural reconstruction of the positive electrode surface can occur which can contribute to impedance growth and capacity loss.[3,4] The by-products of oxidation at the positive electrode can migrate to the negative electrode surface and be reduced there.[8,9] Such reactions can lead to the consumption of lithium ions from the electrolyte, (to maintain charge neutrality in the electrolyte), a reduction in lithium inventory, as well as a thickening of the negative electrode solid electrolyte interface (SEI) which together ultimately cause cell-failure.[10,11] These processes are accelerated by higher charging potentials and higher temperatures.

Methods such as modification of the positive electrode surface with coatings or dopants[12,13] and/or modification of electrolyte with electrolyte additives have been developed to improve the lifetime of Li-ion cells operated to high potential.[14–17] Ma et al. showed that the selection of electrolyte additives can significantly impact the performance of lithium ion cells. Ma et al. showed that the addition of 2 wt% prop-1-ene-1,3 sultone (PES) +1 wt% tris (trimethylsilyl) phosphite (TTSPi) + 1 wt% methylene methane disulfonate (MMDS) or 1 wt% ethylene sulfate (DTD) in 1 M $LiPF_6$ in ethylene carbonate: ethyl methyl carbonate (3:7 by weight) (these electrolytes are called PES211M (when MMDS is used) or PES211D (when DTD is used)) improved capacity retention and suppressed impedance growth in $Li[Ni_{0.42}Mn_{0.42}Co_{0.16}]O_2$ (NMC442)/graphite pouch cells were operated to 4.4 V and above.[14] Many studies of the effectiveness of coatings on and dopants in positive electrode materials have been carried out in half cell coin cells with standard electrolytes (no additives).[18–27] Such results cannot be simply extrapolated to full cells especially when electrolyte additives are used. For example, J. Xia et al.[28] and K.J Nelson et al.[29] showed that $LaPO_4$-coatings on $Li[Ni_{0.42}Mn_{0.42}Co_{0.16}]O_2$ provided a limited benefit when state-of-the-art electrolyte additives were used. R. S. Arumugam et al.[3] showed that an $Al_2O_3$ coating on $Li[Ni_{0.6}Mn_{0.2}Co_{0.2}]O_2$ (NMC622) acts synergistically with PES211D electrolyte at 4.4 V. It is therefore important to combine surface modification techniques and electrolyte additives to improve the life-time of Li-ion batteries with high upper cutoff voltages.

Figures 1B shows scanning electron microscope (SEM) images of commercial samples of $Li[Ni_{0.5}Mn_{0.3}Co_{0.2}]O_2$ (NMC532) without a surface coating (UC-532), while Figures 1b shows an expanded view of the particle surfaces. Figures 1B and 1b show that NMC532

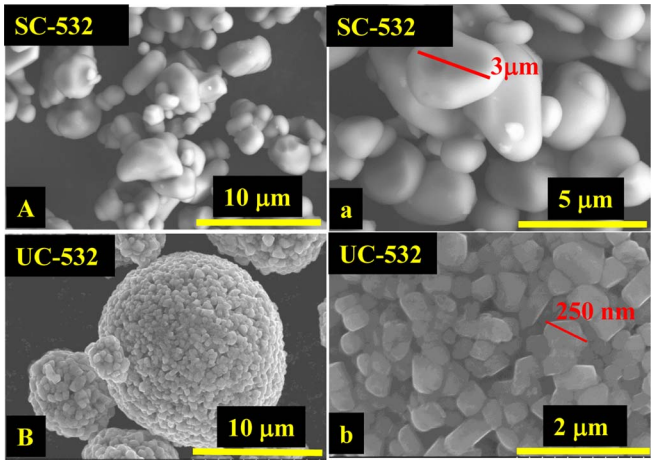


**Figure 1.** SEM images of a commercial single-crystal $Li[Ni_{0.5}Mn_{0.3}Co_{0.2}]O_2$ (NMC532) (called SC-532) material with large grain size of ~3 μm (A, a), SEM images of commercial polycrystalline (NMC532) without coating (UC-532) (B, b).

*Electrochemical Society Fellow.
[z]E-mail: jeff.dahn@dal.ca

typically has large secondary particles around 15 μm made of agglomerates of small crystals of ~200–400 nm. For $Al_2O_3$ coated NMC532 (AC-532), $Al_2O_3$ particles are usually around 40 nm scattered on the surface of the NMC532 particles.[19,20] Thick coatings (higher than 3 wt%) with inactive oxides on NMC materials significantly decrease the energy density and rate capability of cells and thus coating is often incomplete.[19,20]

Figures 1A and 1a show the SEM images of a commercial single-crystal NMC532 (SC-532) material with large grain size of ~3 μm, which will be carefully examined in this work. There are many reasons why single crystal NMC materials could be superior to the "standard" polycrystalline materials shown in Figures 1B and 1C. For example, commercial $LiCoO_2$ (LCO) materials usually have large particle size (primary) of 6~14 μm ($d_{50}$) with a very smooth surface.[30] J. Jiang et al. showed that $Li_{0.5}CoO_2$ with larger grain size had a higher onset temperature for self-heating, as measured by accelerating rate calorimetry in the presence of electrolyte, which indicates the larger the particle size, the lower the reactivity of $Li_{0.5}CoO_2$ with the electrolyte and hence the better the thermal stability of charged cells.[31] Hence, it may be beneficial for NMC materials to have large grain size (2–10 μm) like LCO for better electrolyte stability at high voltages. This work will thoroughly study the pros and cons of single-crystal NMC532 in comparison to polycrystalline $Al_2O_3$-coated (AC-532) and polycrystalline un-coated NMC532 (UC-532). Pouch cells using artificial graphite as the negative electrode, with various electrolyte additives, were used for a complete evaluation of the electrochemical performance.

L. Wang et al. recently showed the synthesis of single crystal NMC622 using a hydrothermal method together with multi-step sintering, which demonstrated that the optimal grain size that could be achieved was ~800 nm.[32] To our knowledge, there have been no reports in the academic literature showing that single crystal NMC with grain size around 3 μm was successfully synthesized with good electrochemical performance. However, single crystal NMC materials are now available from a number of suppliers. There are a few patents from industry regarding the synthesis of single crystal NMC.[33,34] In this work, the key synthesis steps of single crystal NMC will be discussed and further details will be reported later. This work describes a class of NMC-based positive electrode materials that may be suitable for lithium ion cells with high energy density and long lifetime.

## Experimental

Reagents used for the synthesis of single crystal NMC532 included nickel (II) sulfate hexahydrate ($NiSO_4 \bullet 6H_2O$, 98%, Alfa Aesar), manganese sulfate monohydrate ($MnSO_4 \bullet H_2O$, 98%, Alfa Aesar), sodium hydroxide (NaOH, 98%, Alfa Aesar), ammonium hydroxide ($NH_4OH$, 28.0–30.0%, Sigma-Aldrich). All aqueous solutions used in the precursor synthesis were prepared with deionized (DI) water which was de-aerated by boiling for 10 minutes.

Reagents used for coin cells and pouch cells included 1:2 v/v ethylene carbonate:diethyl carbonate (EC:DEC, BASF, purity 99.99%), 3:7 w/w ethylene carbonate:ethyl methyl carbonate (EC:EMC, BASF, purity 99.99%, water content <20 ppm) and lithium hexafluorophosphate ($LiPF_6$, BASF, purity 99.9%, water content 14 ppm). Vinylene carbonate (VC, BASF, purity 99.97%, water content <100 ppm), pyridine-boron trifluoride (PBF, 3 M, purity >99%),[35] prop-1-ene-1,3-sultone (PES, Lianchuang Medicinal Chemistry Co., purity 98.20%), ethylene sulfate (DTD, Sigma Aldrich, purity 98%), tris (trimethylsilyl) phosphite (TTSPi, TCI America, purity >95%) and fluoroethylene carbonate (FEC, BASF, purity 99.94%,), were used as electrolyte additives.

***Scanning electron microscopy imaging.***—A Hitachi S-4700 Scanning Electron Microscope (SEM) equipped with an 80 $mm^2$ silicon drifted detector (Oxford Instruments) was used to study the morphology of the commercial SC-532, AC-532 and UC-532 materials as shown in Figure 1. The AC-532 and UC-532 materials were studied after being recovered from fresh electrodes (taken from dry–no electrolyte - cells) as access to the commercial powders was not possible. Samples were prepared by mounting the powder on adhesive carbon tape prior to imaging. The images of samples were collected with an accelerating voltage of 5 kV and current of 10 μA. A NanoScience Phenom Pro G2 Desktop Scanning Electron Microscope (SEM) was used to study the morphology of the samples synthesized at Dalhousie University.

***Electron backscatter diffraction (EBSD).***—Samples of SC-532 were prepared by an ion beam cross-section polisher (JEOL IB-09010CP) at the Canadian Centre for Electron Microscopy (CCEM). The SC-532 powder sample was first embedded in a graphite block with carbon paint (PELCO) and then the cross-section of the block was milled by the cross-section polisher with an Ar ion beam. Electron backscatter diffraction (EBSD) mapping was carried out using a JEOL JSM-7000F SEM at CCEM. Step size of the EBSD maps were 250 nm (each pixel is 250 nm × 250 nm).

***Powder X-ray diffraction (XRD).***—Powder X-ray diffraction (XRD) was carried out using a Siemens D5000 diffractometer equipped with a Cu target X-ray tube and a diffracted beam monochromator. Diffraction patterns were collected in the scattering angle (2θ) range of 15–70° at 0.025° intervals with a dwell time of 15 s. A 0.5° divergence slit, 0.5° anti-scattering slit and 0.05 mm receiving slit were used for high resolution measurements. Measurements on a NIST sample (standard reference material 1976) of highly crystalline corundum under the same measurement conditions showed a full width half maximum of the (113) peak of 0.024 degree for the $K\alpha_1$ peak (centered at 43.35°), demonstrating the instrumental resolution at this diffraction angle

***Coin cells.***—Single side coated electrodes were punched (1.2 cm diameter) from the ends of the NMC532 electrodes extracted from the dry (no electrolyte) pouch cells which are described in the "pouch cell" section below. The punched electrodes were dried overnight at 120°C in a vacuum oven before use. The electrolyte used was 1.0 M $LiPF_6$ in EC:DEC. The separators used were one Celgard 2320 (Celgard) next to the lithium electrode and one polypropylene blown-microfiber separator (3 M) adjacent to the positive electrode. Galvanostatic charge/discharge cycling using standard 2325 coin cells with lithium metal as the negative electrode was done using an E-One Moli Energy Canada battery testing system. All the cells were tested with a current density of 10 mA/g (~C/20) for 5 cycles between 3.0–4.3, 4.4 or 4.5 V (vs. $Li/Li^+$), respectively, at 30°C. Separate cells were used for each potential range.

***Synthesis of single crystal NMC532.***—$Ni_{0.5}Mn_{0.3}Co_{0.2}(OH)_2$ precursors were prepared via co-precipitation in a continuously stirred tank reactor (CSTR) (Brunswick Scientific/Eppendorf BioFlo 310).[36] The details of the synthesis of similar precursors has been described by J. Li et al.[37,38] The dried precursors were mixed with a stoichiometric equivalent of $Li_2CO_3$ (from Umicore, >99%) by hand grinding using a mortar and pestle until a homogenous consistency was achieved (about 10–15 minutes). Samples with Li/transition metal (TM) ratios of 1.15, 1.20 and 1.25 were prepared. The powder mixtures were sintered in air in a box furnace at 930, 950, 970, 990 or 1020°C for 12 hours, with an initial heating rate of 10°C/min and a final cooling rate of 10°C/min for all samples. The final products were ground and passed through a 75 μm sieve prior to characterization.

***Pouch cells.***—402035 size machine-made SC-532 and UC-532 /graphite pouch cells (200 mAh) were obtained dry (no electrolyte) from LiFun Technology (Xinma Industry Zone, Golden Dragon Road, Tianyuan District, Zhuzhou City, Hunan Province, PRC, 412000). 402035 size cells with AC-532 were received dry (no electrolyte) from Umicore (Cheonan, Korea). All cells used the same artificial graphite negative electrode material (Kaijin AML-400 from Kaijin, China). All cells were vacuum sealed before they were shipped to Canada. The detailed surface properties of SC-532 material are unknown and

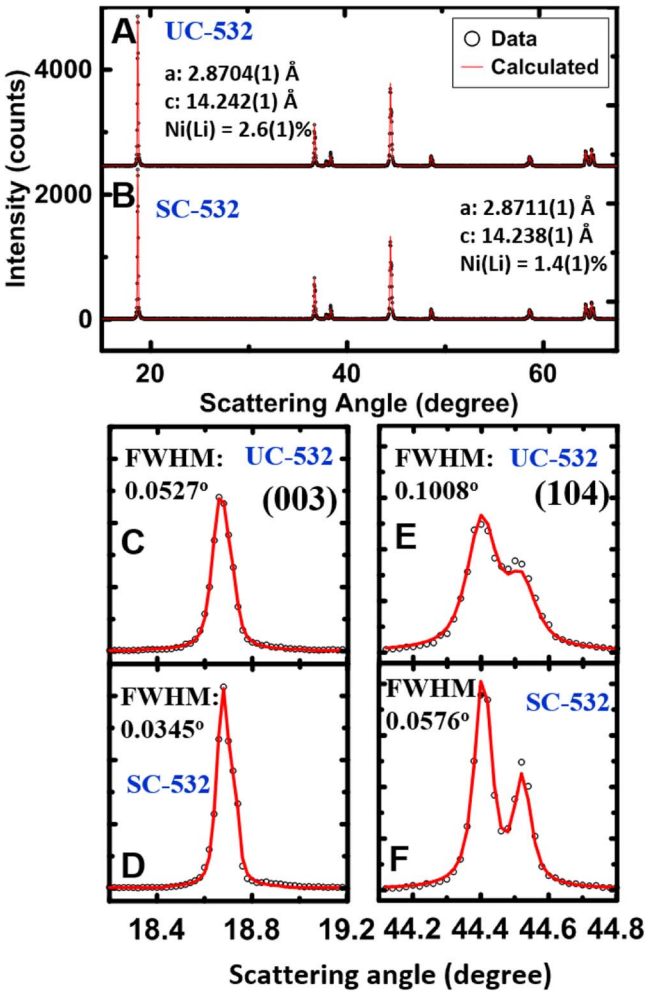


**Figure 2.** XRD patterns of the UC-532 (A) and SC-532 (B). An expanded view of the (003) reflection for UC-532 (C) and SC-532 (D), and an expanded view of the (104) reflection for UC-532 (E) and SC-532 (F). The black dots show the measured data points and the red solid lines show the fits to the data using Rietveld refinement.

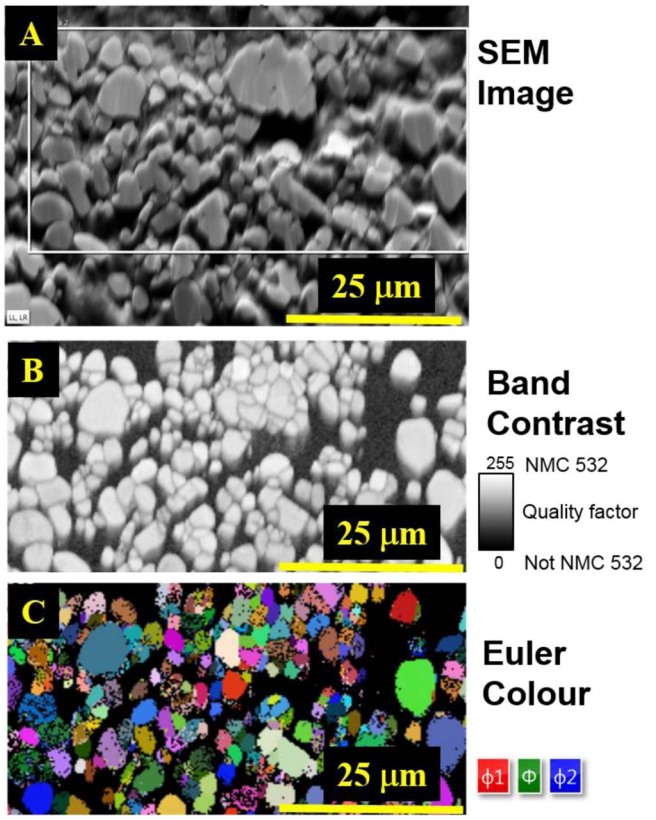


**Figure 3.** Cross-sectional SEM images of SC-532 samples (A), while the white rectangular box indicates the region where the EBSD mapping was carried out. The band contrast EBSD map (B) and the EBSD orientation map (C) in the selected region of the SC-532 sample. φ1, φ, and φ2 are angles relative to the SEM-axis stage. Each color indicates a specific crystal orientation of the grains.

will be analyzed in the future. The SC-532, UC-532 and AC-532 cells were balanced so that they could be charged to 4.7, 4.5 and 4.5 V, respectively, without any lithium plating. Figure S1a in the supporting information shows an example of the positive and negative voltage (vs. Li) and full cell voltage as a function of cell capacity for the SC-532 cells from dV/dQ analysis.[39]

For electrolyte filling, the cells were cut open below the heat seal and placed in a heated vacuum oven at 100°C overnight (approximately 14 hours) to remove residual water. After drying, the cells were directly transferred to an argon-filled glove box without exposure to ambient air, where they were filled with 0.90 g electrolyte. The control electrolyte was 1 M $LiPF_6$ in 3:7 v:v EC:EMC. Electrolyte additives used in this work were VC, FEC, PBF, PES, TTSPi and DTD. The combinations of the above additives in control electrolyte studied were 2 wt% VC (2VC), 2 wt% PES (2PES), 1 wt% PBF (1PBF) and 2 wt% PES + 1 wt% TTSPi + 1 wt% DTD (PES211). 5 wt% FEC in 1 M $LiPF_6$ in EMC (called Q5FEC here) was also studied. Once cells were filled with electrolyte, they were sealed with a compact vacuum sealer (MSK-115V, MTI Corp.) to 94% of full vacuum (−95.2 kPa gauge pressure or 6.1 kPa absolute pressure) with a 6 second sealing time at 165°C.

All cells were placed in a temperature-controlled box at 40. ± 0.1°C and held at 1.5 V for 24 hours to ensure complete wetting. Then cells were charged at C/20 to 3.8 V using a Maccor series 4000 automated test system (Maccor Inc.), where C/20 is the current required to complete a full charge (to 4.4 V) or discharge in 20 hours. The cells were transferred back to an argon-filled glove box and cut open under the previous seal to release any gas that was produced. The cells were then vacuum sealed again as previously described. A second degas was performed after the charge to 4.4 V.

***Ultra-high precision coulometry (UHPC).***—The coulombic efficiency of cells was measured using the ultra high precision chargers at Dalhousie University described in Reference 40. The cells after formation were tested at C/20 for 16 cycles between 3 and 4.4 V. The cells were placed at 40. ± 0.1°C in temperature-controlled boxes during the tests.

***Long term cycling.***—The cells were tested for long term cycling with a C/2 rate assuming a capacity of 200 mAh between 3 and 4.4 V. A cycle at C/20 rate every 50 cycles was included. The cells were held at the top of charge until the current reached C/20 during each cycle. The tests were made at 40. or 55. ± 0.1°C in temperature-controlled boxes. Neware (Shenzen, China) chargers were used for these tests.

***In-situ gas measurement.***—The gas produced in cells due to electrolyte decomposition during testing was measured using Archimedes' principle.[41] A strain gauge load cell was used to measure changes in the buoyant force of cells submerged in mechanical pump oil kept at a steady temperature as the pouch cells were charged and discharged. A detailed account of this method was described by Aiken et al.[41] SC-532 and AC-532 cells with PES211 electrolyte after formation were first tested between 3–4.3 V for one cycle and then charged and held at 4.4, 4.5 and 4.6 V for 100 h subsequently. The current used

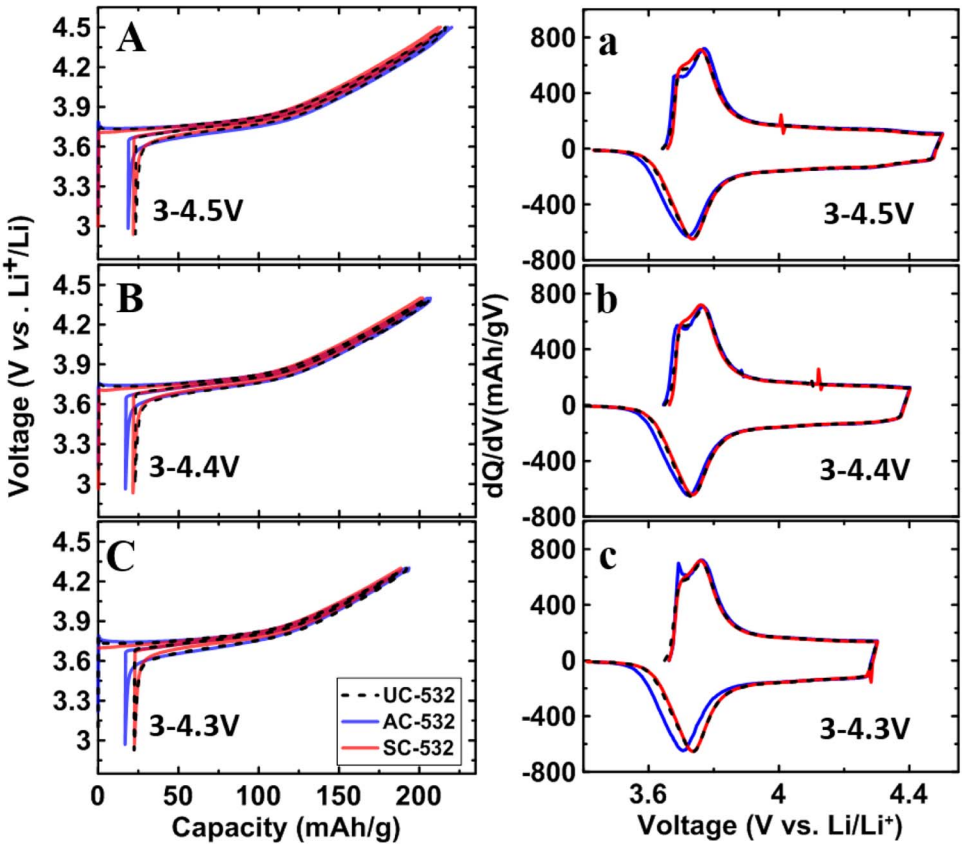


**Figure 4.** Voltage as a function of specific capacity measured between 3–4.5 (A), 4.4 (B) and 4.3 V (C), respectively, from coin cell half cells with a current of 10 mA/g (∼C/20 rate) for SC-532, AC-532 and UC-532 materials. The measurements were made at 30°C. Differential capacity as a function of cell voltage measured between 3–4.5 (a), 4.4 (b) and 4.3 V (c) respectively. The dashed black lines show the results for UC-532 cells, blue solid lines show the results for AC-532 cells and red solid lines show the results for SC-532 cells.

during testing was ∼C/20 calculated with capacity measured between 3–4.3 V and the tests were made at 40°C. The changes in the volume of the cells during testing were tracked as a function of time.

***Isothermal microcalorimetry.—***Cells used for isothermal microcalorimetry measurements underwent formation, then were transferred into a TAM III Microcalorimeter (TA Instruments: stability ± 0.0001°C, accuracy ± 1 μW, precision ± 1 nW) at 40.0°C and connected to a Maccor 4000 series cycler. The baseline drift over the course of the experiments did not exceed ± 0.5 μW. All specifications and information regarding microcalorimetry calibration, cell connections and operation procedures can be found in previous literature.[42] The AC-532 cells for this study used natural graphite (grade BTR918H from BTR New Materials Technology, China) as the negative electrode due to limited availability of the original AC-532 cells. Cells were cycled four times at a C/20 rate between 2.8 V and 4.2 V to ensure a well formed, stable negative electrode SEI and were then cycled between 3.9 V and different upper cutoff limits: 4.2 V, 4.3 V (twice), 4.4 V (twice) and again to 4.2 V (twice) at 1 mA (SC-532 cells) or 1.5 mA (AC-532 cells) to investigate the performance and the parasitic heat flow in different voltage ranges. The parasitic heat flows in this report have been scaled according the capacity of the cells tested to ensure a fair comparison. A description of the analysis techniques is provided in the results and discussions section.

***Thermogravimetric analysis/mass spectrometry (TGA-MS).—***The cells with PES211 electrolyte after formation were first charged to different upper cutoff voltages of 4.2, 4.4 or 4.6 V respectively with a C/10 rate at 40°C and held at the upper cutoff voltage for 10 h. The cells were then quickly transferred to an Ar-filled glove box and disassembled carefully before any obvious cell voltage drop. The charged positive electrodes were extracted from the pouch cells and were repeatedly rinsed with dimethyl carbonate (DMC) six times to ensure a minimal amount of electrolyte remained in the electrode. Charged positive electrode powders were then scratched off the rinsed electrodes and transferred in air as quickly as possible for TGA/MS experiments to minimize air exposure. A TA-instruments SDT-Q600, coupled to a TA-instruments Discovery MS mass spectrometer was used for these experiments. About 80 mg of the electrode material from each cell was loaded for each test. During the experiment, the sample was first set to stay at room temperature for 11 minutes with a flow of argon at 400 mL/min. Then the samples were heated to 350°C at 10°C/min with a flow of argon at 100 mL/min while ions with m/z = 32 (corresponding to $O_2$) were monitored by the mass spectrometer.

## Results and Discussion

Figures 2A and 2B show the XRD patterns of the UC-532 and SC-532 respectively, where the black dots show the measured data points and the red solid lines show the fits to the data using Rietveld refinement. The calculation assumed a single hexagonal layered phase (α-$NaFeO_2$-type structure described in the R-3m space group) with Li on the 3a sites (lithium layer), transition metals on the 3b sites (transition metal layer) and oxygen on the 6c sites. The exchange of Ni and Li atoms between 3a and 3b sites was allowed with constraints that the stoichiometry of the samples was fixed.[43] The refinement results showed that the lattice constants of UC-532 and SC-532 were very similar as displayed in each panel. Figures 2C and 2D show an expanded view of the (003) reflections of UC-532 and SC-532, respectively, while Figures 2E and 2F show the (104) reflection, accordingly. The full width half maximum (FWHM) of each peak is displayed in the corresponding panels. Figure 2F shows a clear separation between

**Table I. Summary of the reversible and irreversible capacities of the SC-532, AC-532 and UC-532 with different upper cutoff voltages. The number in the brackets show the error of the last digit.**

| 4.3 V | 1st CC (mAh/g) | 1st DC (mAh/g) | IRC (mAh/g) | IRC (%) |
|---|---|---|---|---|
| AC | 191.6(2) | 174.6(1) | 17.2(2) | 8.8(1) |
| UC | 191.6(5) | 169.5(2) | 22.1(2) | 11.5(1) |
| SC | 187(1) | 165.6(3) | 21.9(7) | 11.6(4) |
| 4.4 V | 1st CC (mAh/g) | 1st DC (mAh/g) | IRC (mAh/g) | IRC (%) |
| AC | 204.9 | 188.1 | 16.8 | 8.2 |
| UC | 204.4(1) | 181.7(2) | 22.7(2) | 11.1(1) |
| SC | 201.3(5) | 179.2(1) | 22.1(5) | 10.9(2) |
| 4.5 V | 1st CC (mAh/g) | 1st DC (mAh/g) | IRC (mAh/g) | IRC (%) |
| AC | 217.5(3) | 199.2(1) | 18.2(4) | 8.4(2) |
| UC | 215.9(5) | 192.7(4) | 23.2(1) | 10.7(1) |
| SC | 211.8(1) | 189.9(1) | 21.9(1) | 10.4(1) |

the $K\alpha_1$ and $K\alpha_2$ peaks of the (104) reflection in the SC-532 sample with much narrower peak width compared to the UC-532 sample (Figure 2E). The calculated FWHM of the (104) $K\alpha_1$ peak of SC-532 is 0.0576° which is much smaller than that of the corresponding peak of the UC-532 sample (0.101°). This indicates that SC-532 has a much larger crystallite size compared to UC-532.

To confirm if the SC-532 particles were actually single crystals, powder samples were embedded in a graphite block with carbon paint and then sectioned and milled with an Ar-ion beam for electron backscatter diffraction (EBSD) mapping. Figure 3A shows the cross-sectional SEM image of an SC-532 sample, while the white rectangular box indicates the region where the EBSD mapping was carried out. Figure 3B shows an 8-bit quality factor image of how well the measured crystals compared to a reference lattice of NMC532. Grain boundaries would not fit the reference perfectly and thus would show up black (in addition to the carbon substrate). This technique is useful in determining whether particles are polycrystalline or monocrystalline (single crystal). Figure 3B shows that some large particles consisted of a few smaller grains while most the particles were single grains. Figure S2 in the supporting information shows the grain size distribution diagram, and the average grain size was around 2–3 μm. Figure 3C shows a map of the Euler angles taken using EBSD in the selected region of the SC-532 samples. The three angles φ1, φ, and φ2 can be understood as a series of rotations required to coincide the crystal's crystallographic lattice with the reference axes. In other words, the orientation of the particles can be compared to a chosen reference frame indicating a relative crystal orientation of the grains. Figure 3c shows multiple orientations within the large particles indicating that some of the large particles (∼10–15 μm size) contain multiple crystallites while most of the particles were single grains with large crystallite size of ∼2–3 μm, this material is called single crystal NMC.

Figures 4A, 4B and 4C show cell potential, V, as a function of specific capacity, Q, measured between 3–4.5, 3–4.4 and 3–4.3 V, respectively, from coin type half cells. The specific current used was 10 mA/g, corresponding to an approximate C/20 rate, and the test temperature was 30 +/−0.1°C. Figures 4a, 4b and 4c show the corresponding dQ/dV vs. V plots for the same samples. The dashed black lines show the results for UC-532, blue solid lines show the results for AC-532 and the red solid lines show the results for SC-532. Figure 4 shows that the dQ/dV curves of UC-532, AC-532 and SC-532 are very similar. Table I shows a summary of the reversible and irreversible capacities of the three materials when charged to 4.3, 4.4 or 4.5 V vs $Li/Li^+$.

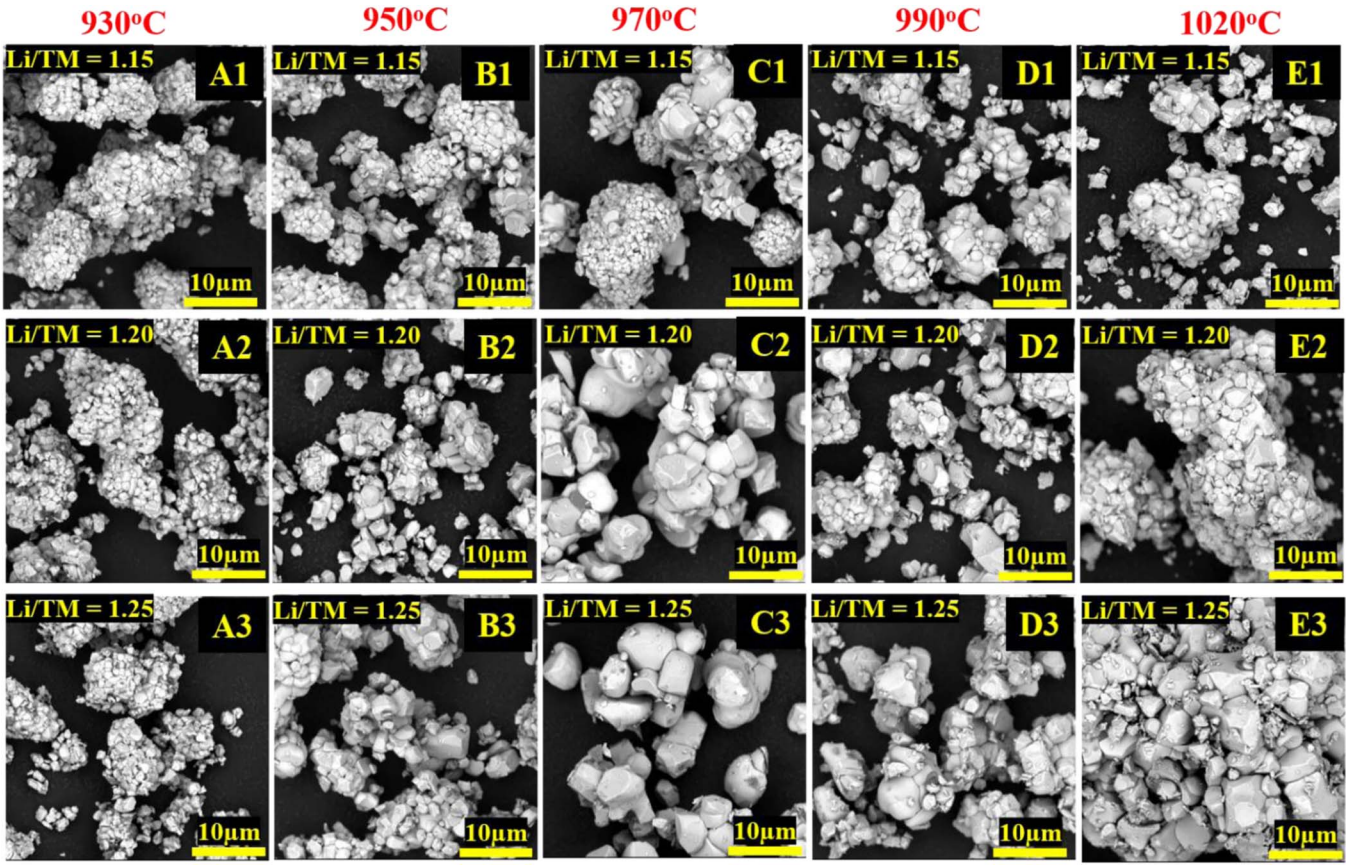


**Figure 5.** SEM images of samples with a Li/TM ratio of 1.15 (A1), 1.20 (A2) and 1.25 (A3) made at 930°C. SEM images of samples with Li/TM of 1.15 (B1), 1.20 (B2) and 1.25 (B3) made at 950°C. SEM images of samples with Li/TM of 1.15 (C1), 1.20 (C2) and 1.25 (C3) made at 970°C. SEM images of samples with Li/TM of 1.15 (D1), 1.20 (D2) and 1.25 (D3) made at 990°C. SEM images of samples with Li/TM of 1.15 (E1), 1.20 (E2) and 1.25 (E3) made at 1020°C.

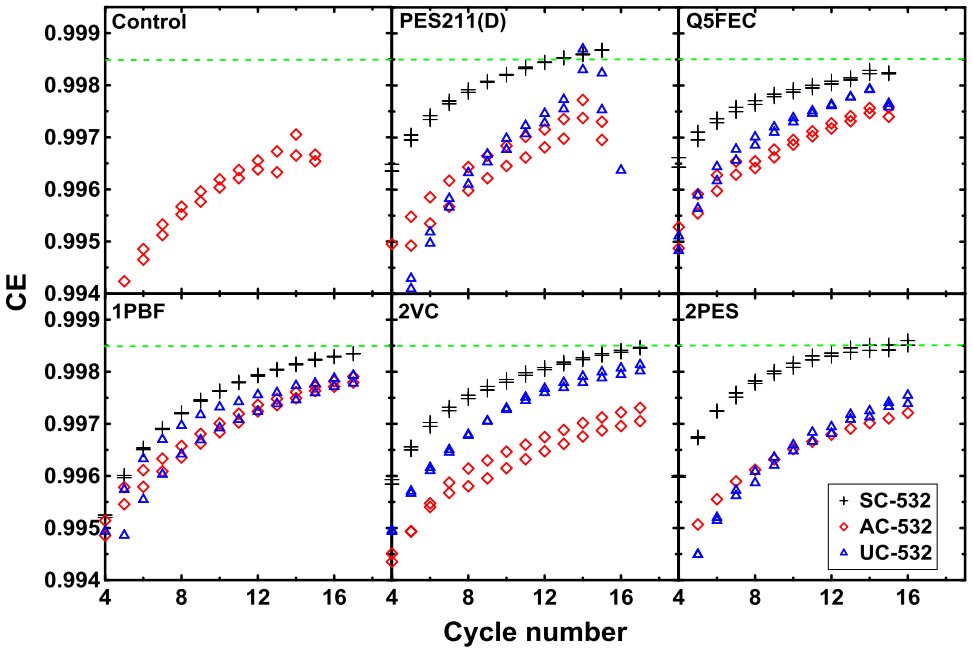


**Figure 6.** The CE of SC-532, AC-532 and UC-532/graphite pouch cells as a function of cycle number with control, PES211, Q5FEC, 1PBF, 2VC and 2PES electrolytes tested between 3–4.4 V at 40°C using currents corresponding to C/20.

Table I shows that AC-532 has the highest reversible capacity (1st discharge capacity) of 174.6(1), 188.1 and 199.2(1) mAh/g between 3–4.3, 4.4 and 4.5 V, respectively compared to those of UC-532 and SC-532. AC-532 and UC-532 were from different manufacturers, and this may explain why UC-532 had lower specific capacity compared to AC-532. Table I also shows that SC-532 has a reversible specific capacity of 165.6(2), 179.2(1) and 189.9(1) mAh/g between 3–4.3, 4.4 and 4.5 V, respectively, which is about 9 mAh/g less than that of AC-532 at each upper cutoff potential. This is a rather large penalty.

The authors were curious to learn how to synthesize single crystal NMC532. After reading a patent (Reference 30) it was clear how single crystal materials could be made. $Ni_{0.5}Mn_{0.3}Co_{0.2}(OH)_2$ precursors with an average particle size around 10 μm were first prepared via the co-precipitation method.[37,38] The dried precursor was mixed with a desired stoichiometric amount of $Li_2CO_3$ by mechanical grinding, and samples with Li/TM ratios of 1.15, 1.20 and 1.25 were prepared. Different powder mixtures were sintered in a box furnace at 930, 950, 970, 990 or 1020°C, respectively, for 12 hours in air. Figures 5A, 5B, 5C, 5D and 5E (columns) show the SEM images of samples made at 930, 950, 970, 990 and 1020°C respectively, while the numbers 1, 2 and 3 in the labels of each column indicate that the Li/TM ratio in the sample was 1.15, 1.20 and 1.25 respectively. For instance, Figures 5A1, 5A2 and 5A3 show the SEM images of samples with Li/TM ratios of 1.15, 1.20 and 1.25, respectively, made at 930°C. Figure 5 shows that the grain size increased with increasing Li/TM ratio at the same temperature. For instance, Figure 5C1 shows that a few large grains of ∼2 μm size appeared at 970°C while most of the grains were about 500 nm in size when the Li/TM ratio was 1.15. Figure 5C2 shows that most of the grains appeared with a large size of around 2–6 μm when the Li/TM ratio increased to 1.2, while Figure 5C3 shows the grain sizes were mostly around 4–8 μm when the Li/TM ratio was 1.25. When the sintering temperature was equal to and below 970°C, the grain size increased with the increase of sintering temperature when the Li/TM ratio was fixed. For instance, Figures 5A2, 5B2 and 5C2 show the average grain size increased from ∼500 nm to ∼1 μm to ∼4 μm when the sintering temperature increased from 930 to 950 to 970°C respectively. When the sintering temperature increased above 970°C, the grain size did not show a continuous size increase as a function of sintering temperature. This is because significant lithium loss occurred at extremely high temperatures.[44] Lithium loss is commonly observed in the synthesis of polycrystalline NMC materials and is normally compensated for by adding some excess lithium (5%) during synthesis.[37] The synthesis conditions needed to optimize electrochemical performance will be discussed in a separate report. Overall, Figure 5 shows that the key to the synthesis of single crystal NMC materials with large grain size is to tune the sintering temperature and the Li/TM ratio. Rapid crystallite growth appears at about 970°C and Li/TM ratios near 1.2 and 1.25.

Figure 6 shows the coulombic efficiency (CE) of SC-532, AC-532 and UC-532/graphite pouch cells as a function of cycle number with control, PES211, Q5FEC, 1PBF, 2VC and 2PES electrolytes tested between 3 and 4.4 V at 40°C. The currents used corresponded to a C/20 rate. Duplicate cells were tested in each case which is why there are pairs of symbols in each panel. For simplicity, the type of positive electrode material will be used to refer to the type of pouch cell. Figure 6 shows that the CE of SC-532 cells was always better than that of the corresponding AC-532 and UC-532 cells except when the control electrolyte (no electrolyte additives) was used. Figure S3 in the supporting information shows the CE of SC-532, AC-532 and UC-532 cells as a function of cycle number in the same graph with a less magnified scale so that the data for SC-532 and AC-532 can be observed. Figure S3 shows that the CE of SC-532 and UC-532 cells with control electrolyte is much worse than that of AC-532 cells. However, Figure 6 shows that SC-532 cells with the various electrolyte additive combinations showed much better CE than those of the SC-532 cells with control electrolyte. Additionally, Figure 6 shows that SC-532 cells with PES211 electrolyte exhibited the best CE of 0.9987 at the 15th cycle (cells were interrupted by power outage after the 15th cycle) which suggests that SC-532 cells with PES211 should have the longest lifetime. This CE of 0.9987 at the 15th cycle is the highest that has been measured in this laboratory for any NMC/graphite cell tested between 3–4.4V at C/20 and 40°C.

Figures S4, S5 and S6 show the discharge capacity, the charge end point capacity and the difference between the average charge voltage and the average discharge voltage, ΔV, as a function of cycle number, respectively, for SC-532, AC-532 and UC-532 cells collected during the UHPC experiment. Figure S5 shows that SC-532 cells always exhibited much smaller charge end point capacity slippage than that of the corresponding AC-532 cells except when the control electrolyte was used. This suggests that SC-532 cells create fewer

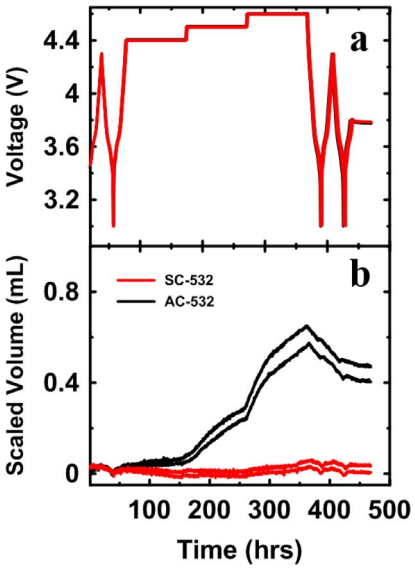


**Figure 7.** The in-situ gas evolution cell voltage as a function of time (a), and the gas volume of SC-532 and AC-532 cells as a function of time (b). The black solid lines show the results for the AC-532 pair cells and the red lines show the results for the SC-532 pair cells.

oxidized species compared to AC-532 cells when combined with the selected electrolyte blends. SC-532 cells with PES211 electrolyte showed the smallest charge end point capacity increase, which was only 4 mAh at cycle 15. In fact, all the properties (discharge capacity, $\Delta V$, charge end point capacity and CE) corresponding to SC-532 cells with PES211 were superior to those of cells with the other additive blends. This again indicates that SC-532 cells with PES211 electrolyte should have the best cycle life.

To further investigate the electrolyte stability at the SC-532 and AC-532 positive electrode surface, cells with PES211 electrolyte were charged and held at 4.4, 4.5 and 4.6 V for 100 h while the volumes of gas produced in the cells due to electrolyte decomposition at high voltages were measured in-situ. The temperature of the experiment was 40.0°C. PES as an electrolyte additive is known to suppress gas production in NMC/graphite cells.[3,14,45] Figure 7b shows the gas volume of SC-532 and AC-532 cells as a function of time while Figure 7a shows the corresponding cell voltage as a function of time. The black solid lines show the results for the AC-532 pair cells and the red lines show the results for the SC-532 pair cells. Figure 7b shows SC-532 cells produced gas volumes of 0.01(1), 0.01(1) and 0.04(1) mL after the holds at 4.4, 4.5 and 4.6 V for 100 h respectively. These are extremely small volumes of gas considering that the initial cell volume was about 2.5 mL. By comparison, AC-532 cells generated 0.07(1), 0.27(3) and 0.62(4) mL gas respectively after holding at the corresponding voltages. Figure 7b shows that SC-532 cells produced negligible amounts of gas after holding at high voltages for 300 h indicating the superior stability of the single crystal NMC532 electrode surface when PES211 electrolyte was used. By contrast, AC-532 cells produced much more gas during the hold at high voltages, which suggests that the aluminum oxide coating does not prevent oxidation of species in the electrolyte at or above 4.4 V.

The SC-532 and AC-532 cells with PES211 electrolyte were also studied with isothermal microcalorimetry to probe the magnitude of the parasitic reactions by separating the parasitic heat flow from the measured heat flow from the cells. When current is applied to a cell, the measured heat flow comes from the voltage polarization, entropy changes in the electrode materials, and the parasitic reactions occurring in the cell.[42,46] Since the entropic heat flow is reversible between charge and discharge, the average parasitic heat flow at each voltage point can be found by taking the average of charge and discharge heat flow and subtracting the average overpotential heat flow. The details of this method was introduced by S. Glazier et al.[47] Figure 8a shows the resulting parasitic heat flow calculation of a sample cell between 3.9 V and 4.2 V. The black lines show the total measured heat flow during charge (solid) and discharge (dashed), the green and blue lines show the overpotential heat flow, and the red line demonstrates the average parasitic heat flow between charge and discharge. During the calorimetry experiments, cells were cycled between 3.9 V and different upper cutoff potentials: 4.2 V, 4.3 V (twice), 4.4 V (twice) and again to 4.2 V (twice) at 1 mA (SC-532 cells) or 1.5 mA (AC-532 cells). These currents corresponded to a C/100 rate for each type of cells. Figure 8b shows a summary of the results by plotting the mean parasitic heat flow over each cycle (the average value of the red curve in Figure 8a) to the various potentials, where the blue and red diamonds show the mean parasitic heat flow for SC-532 and AC-532 pair cells respectively. Figure 8b shows that SC-532 cells have a lower mean parasitic heat flow than AC-532 cells in all voltage ranges, which suggests that SC-532 cells should have longer lifetime than AC-532 cells. This result agrees well with the observation from UHPC and in-situ gas experiments.

Figures 9a, 9b and 9c show the detected oxygen (m/z = 32) intensity released from electrode materials that were held at 4.2, 4.4 and

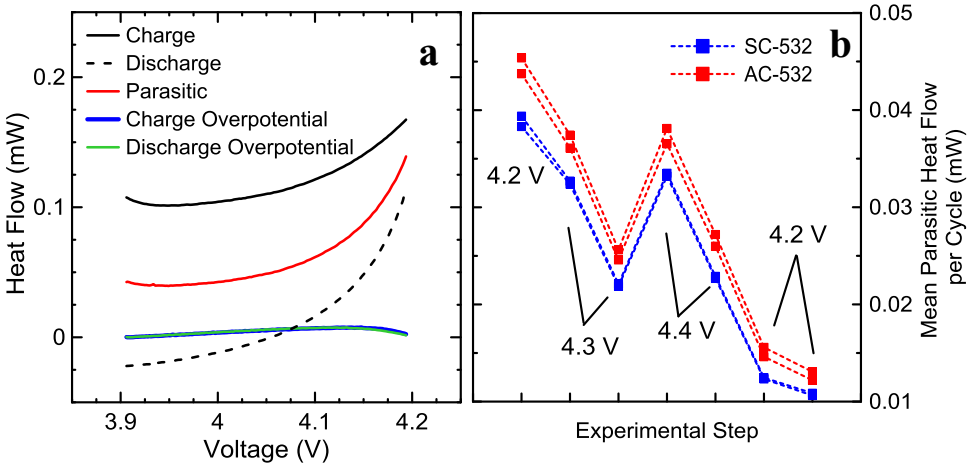


**Figure 8.** The parasitic heat flow calculation of a sample cell between 3.9 V and 4.2 V (a). The black lines show the measured heat flow during charge (solid) and discharge (dashed), the green and blue lines show the overpotential heat flow, and the red line demonstrates the average parasitic heat flow between charge and discharge. The summarizes results which plot the mean parasitic heat flow over each cycle (b), where the blue and red diamonds show the mean parasitic heat flow for SC-532 and AC-532 pair cells, respectively.

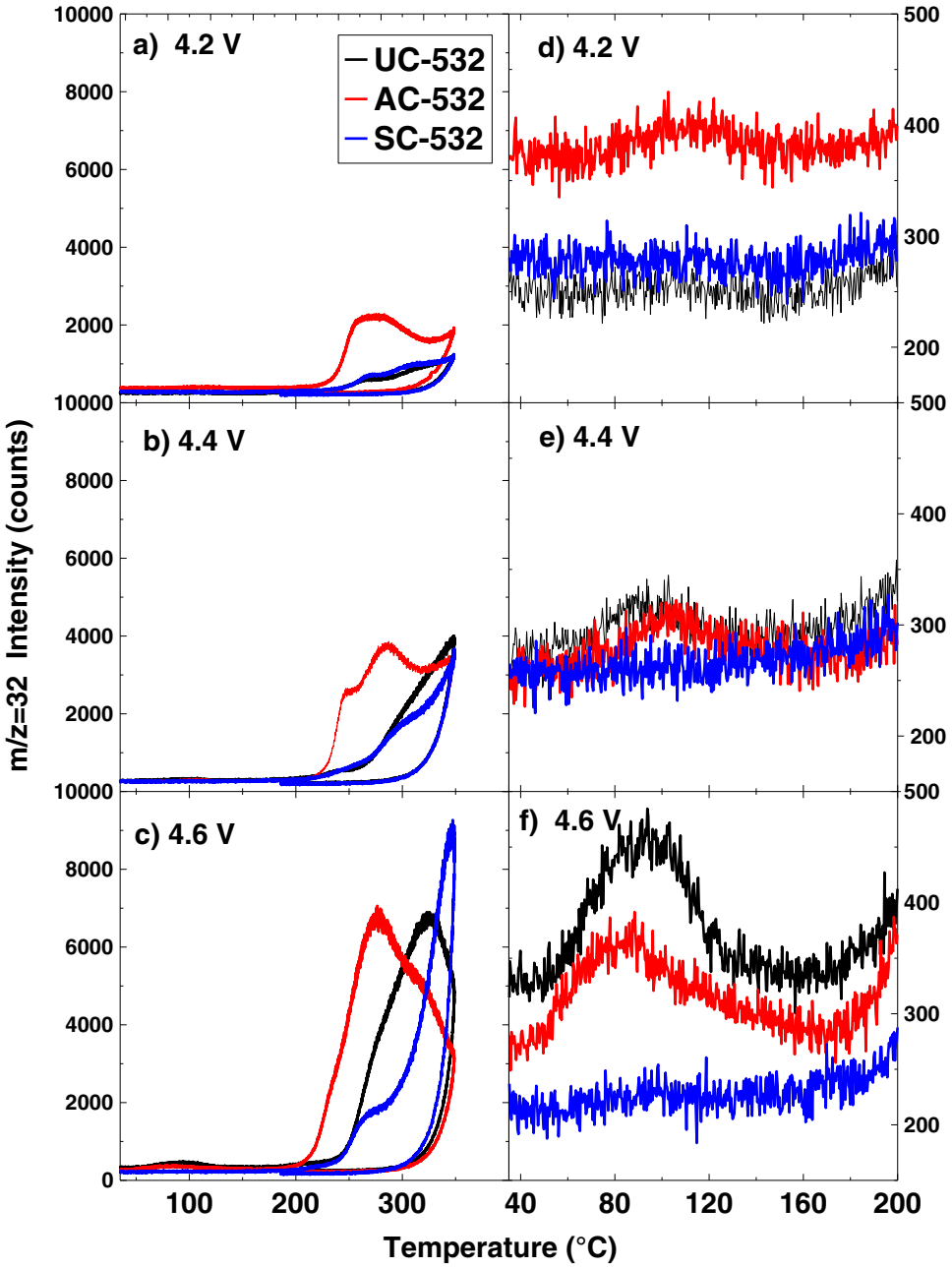


**Figure 9.** The detected oxygen (m/z = 32) intensity of oxygen evolving from NMC532 electrode materials that were held at 4.2 (a, d), 4.4 (b, e) and 4.6 V (c, f), respectively, as a function of temperature from the TGA/MS experiment. Expanded views of the region between 0–200°C are shown in 9d, 9e and 9f respectively. The black, red and blue solid lines show the results for charged UC-532, AC-532 and SC-532 electrode materials respectively.

4.6 V, respectively, as a function of temperature from the TGA/MS experiment, while Figures 9d, 9e and 9f show an expanded view in the region between 0–200°C of the corresponding results shown in Figures 9a, 9b and 9c respectively. The black, red and blue solid lines show the results for charged UC-532, AC-532 and SC-532 electrode materials respectively. Figures 9a, 9b and 9c show that peaks between 200 and 350°C were observed for all the charged electrode materials and the peak intensity increases with increasing of state of charge of the electrode materials (higher upper cutoff voltage of the cells). The release of oxygen from the bulk of the charged materials is associated with the degradation of NMC532 from a layered ($Li_xMO_2$, M = Ni, Mn and Co) structure to a rock-salt ($Li_xM_{1-x}O$) structure.[48] Figures 9d, 9e and 9f show that small oxygen release peaks centered around 80°C were detected for charged AC-532 and UC-532 materials and the peak intensity increased significantly with increasing upper cutoff voltage. By contrast, this peak was not detected for charged SC-532 samples. The origin of this oxygen peak at low temperatures (~80°C) is speculated to be due to oxygen release from the surface of charged AC-532 and UC-532 materials. Presumably, this oxygen release is governed by Arrhenius kinetics so that the rate of surface oxygen release would not be zero even at 40°C, for example. In electrolyte, oxygen atoms or radicals might react with the electrolyte before $O_2$ molecules could form. The absence of the oxygen release peak at 80°C for charged SC-532 samples suggests that charged single crystal NMC532 materials have much better structural stability when interacting with electrolyte than polycrystalline NMC532 materials.

Cells with various electrolyte additives were tested with long term cycling at 40°C using currents corresponding to C/2, assuming a capacity of 200 mAh, between 3 and 4.4 V. Every 50 cycles, one C/20 cycle was performed. During every charge, the cells were held at the

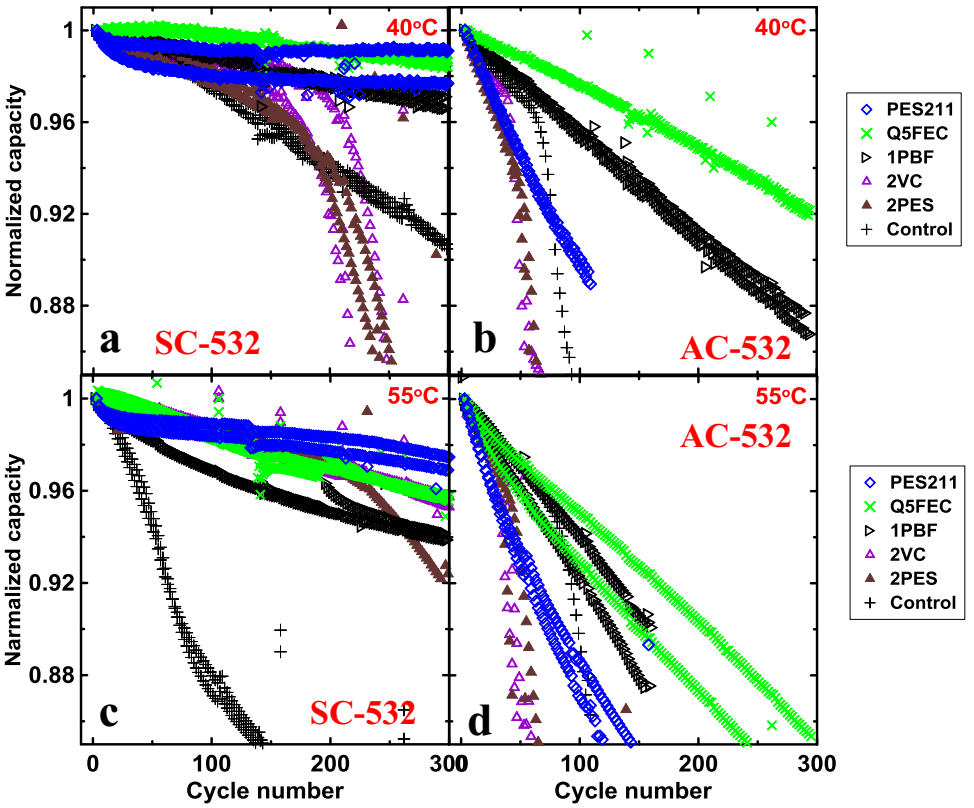


**Figure 10.** The normalized capacity of SC-532 (a) and AC-532 (b) cells, respectively, tested at 40°C (C/2 CCCV between 3.0 and 4.4 V) as a function of cycle number. The normalized capacity of SC-532 (c) and AC-532 (d) cells, respectively, tested at 55°C (C/2 CCCV between 3.0 and 4.4 V) as a function of cycle number.

top of charge until the current reached C/20. Figures 10a and 10b show the normalized capacity of SC-532 and AC-532 cells, respectively, as a function of cycle number while Figures 10c and 10d show the corresponding results for cells tested at 55°C. Figures 10a and 10b show that about 98(±1) % capacity was maintained for SC-532 cells with Q5FEC and PES211 electrolyte after 300 cycles at 40°C, while the best capacity retention for AC-532 cells was ∼92% using Q5FEC electrolyte under the same condition. At 55°C, with accelerated parasitic reaction rates, SC-532 cells with PES211, Q5FEC and 1PBF electrolyte showed more than 94% capacity retention after 300 cycles, while AC-532 cells showed less than 85% retention with any electrolyte tested. Figure 10 shows that SC-532 cells exhibited much better capacity retention than AC-532 cells at both temperatures when the same electrolyte was used. This agrees well with the all the expectations based on the results of high precision coulometry, in-situ gas evolution, microcalorimetry and TGA/MS experiments.

Figures 11a and 11c show the normalized capacity and the corresponding ΔV (differences between the average charge and discharge voltage), respectively, as a function of cycle number for SC-532 cells tested at 40°C with extended cycles while Figures 11b and 11d show the corresponding results for SC-532 cells tested at 55°C. Figure 11a shows that SC-532 cells with PES211 electrolyte exhibited the best capacity retention of ∼97(±1) % after 800 cycles between 3 and 4.4 V at 40°C, while cells with Q5FEC also showed decent capacity retention of ∼96(±1) %. Figure 11c shows that ΔV vs cycle number of SC-532 cells with PES211 electrolyte is very stable after about 200 cycles while a small increase in ΔV from 0.12 V to 0.16 V during cycling was observed for SC-532 cells with Q5FEC electrolyte. Additionally, Figure 11b shows that SC-532 cells tested at 55°C with PES211 and Q5FEC electrolyte exhibited the best capacity retention of ∼89(1)% after about 800 cycles while Figure 11d shows minimal increase of polarization of the corresponding cells at 55°C. It is necessary to point out that the cycling results for SC-532 cells with PES211 electrolyte at both 40 and 55°C are the best ones ever observed in NMC/graphite cells tested between 3 and 4.4 V in this laboratory. Unfortunately, the use of PES211 electrolyte usually leads to large negative electrode charge transfer resistance which means the cells are not suitable for applications requiring high rate charging during operation.[49]

Figure 12 shows the normalized capacity and the corresponding ΔV as a function of cycle number for SC-532 cells with PES211 and Q5FEC tested at 40°C. Figure 12 shows the same cycling results that were presented in Figure 11 with additional cycles–1600 cycles. Figure 12 shows that SC-532 cells with PES211 and Q5FEC electrolyte still retained ∼92% capacity after 1600 cycles at 40°C in over one year of testing.

Finally, Figure S7 shows that the discharge rate capability of SC-532, UC-532 and AC-532 cells with control electrolyte is very similar, at least up to rates as large as C/2. This means that the large single crystals do not impede solid state $Li^+$ ion diffusion dramatically in comparison to the large poly crystalline materials.

## Conclusions

In summary, this work compared a single-crystal NMC532 material with grain size around 2–3 μm to conventional polycrystalline uncoated and $Al_2O_3$-coated NMC532 materials. The key to the synthesis of single crystal NMC532 materials with large grain size appears to be tuning the sintering temperature and Li/TM ratio. Rapid crystallite size growth for NMC532 appeared at sintering temperatures about 970°C and when the Li/TM ratio was above about 1.15.

Half cell tests showed that the SC-532 material had lower specific capacity (about 9 mAh/g) compared to AC-532 and UC-532 materials in the same voltage range. However, it was shown that SC-532 material has far superior stability at high voltage and high temperature leading to SC-532/graphite pouch cells with exceptional capacity retention at 4.4 V. UHPC tests showed that the CE values of SC-532 cells were always better than those of AC-532 and UC-532 cells with the same

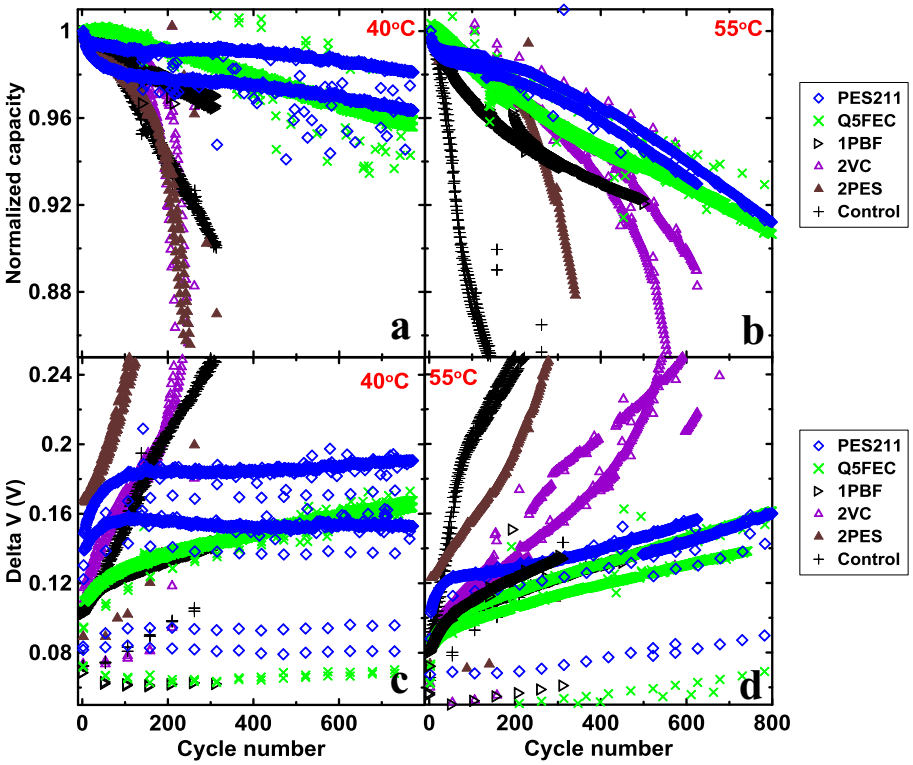


**Figure 11.** The normalized capacity (a) and the corresponding ΔV (difference between the average charge and discharge voltage) (c), respectively, as a function of cycle number for SC-532 cells tested at 40°C (C/2 CCCV between 3.0 and 4.4 V) for 800 cycles. The normalized capacity (b) and the corresponding ΔV (differences between the average charge and discharge voltage) (d), respectively, as a function of cycle number for SC-532 cells tested at 55°C (C/2 CCCV between 3.0 and 4.4 V) for 800 cycles.

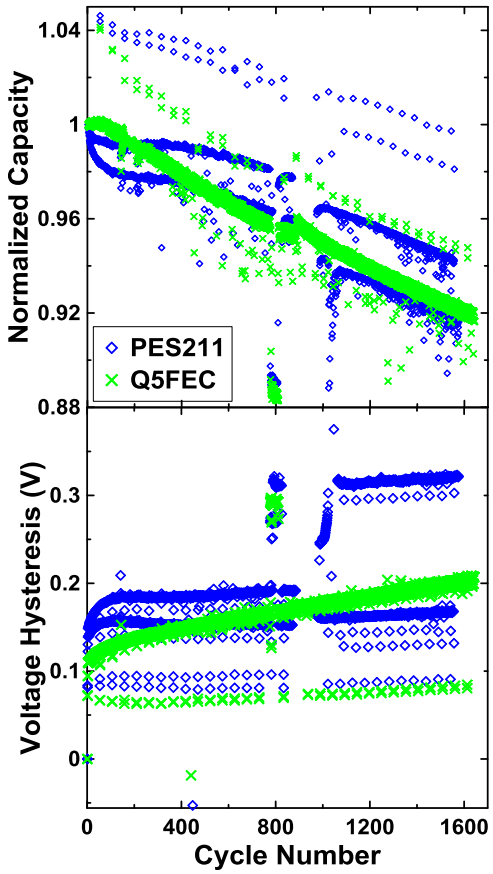


**Figure 12.** The normalized capacity and the corresponding ΔV as a function of cycle number for SC-532 cells tested at 40°C (C/2 CCCV between 3.0 and 4.4 V) for 1600 cycles (over one year of testing shown). Every 50 cycles, a C/20 low rate cycle was applied which explains the additional sets of data points at higher capacity.

electrolyte except for the case of control electrolyte. Additionally, SC-532 cells with PES211 electrolyte exhibited a CE of 0.9987 at the 15th cycle which was highest ever measured in this laboratory for any NMC/graphite cells tested at C/20 between 3 and 4.4 V at 40°C. In-situ gas measurements showed that SC-532 cells with PES211 electrolyte produced negligible amounts of gas during potentiostatic holds at 4.4, 4.5 and 4.6 V for a total time of 300 h at 40°C. By contrast, the AC-532 cells produced substantial amounts of gas in the same experiment. Isothermal microcalorimetry measurements showed that SC-532 cells had a lower mean parasitic heat flow than that of AC-532 cells in all voltage ranges. Moreover, TGA/MS experiments showed release of oxygen around 80°C from charged AC-532 and UC-532 materials whereas it was not detected for charged SC-532 samples. The long-term cycling tests showed that SC-532 cells exhibited much better capacity retention than that of AC-532 cells when the same electrolyte was used in tests carried out at both 40 and 55°C between 3 and 4.4 V with a rate of C/2. SC-532 cells with PES211 electrolyte exhibited excellent capacity retentions of ~92% after 1600 cycles at 40°C.

These results all suggest that the SC-532 material has much better stability against PES211 and other electrolytes at high voltages (4.4 V and above) and high temperature compared to AC-532 and UC-532 materials. It is thus possible to charge SC-532 cells to a relatively higher voltage to compensate for its lower specific capacity while still maintaining excellent lifetime. The use of PES211 electrolyte usually leads to large negative electrode charge transfer resistance and therefore is not recommended for applications requiring high rates during charging.[49] However, for applications where low rates and elevated temperatures are envisaged, such as electrical energy storage from solar panels in hot climates, SC-532 cells with PES211 may be unmatched.

## Acknowledgments

The authors thank NSERC and Tesla Motors for the funding of this work under the auspices of the Industrial Research Chairs program. The authors thank Dr. Jing Li of BASF for providing most of the solvents and electrolyte additives used in this work. The authors thank

Dr. Jens Paulsen and Dr. Xin Xia for providing the AC-532 cells with artificial graphite negative electrodes used in this work and for providing AC-532 electrode materials to LIFUN for production into cells with natural graphite negative electrodes. Finally, the authors thank Dr. Jian Tu of LiFUN for his help in obtaining UC-532 and SC-532 positive electrode materials. The CCEM is a national facility supported by the Canada Foundation for Innovation under the Major Science Initiative program, NSERC and McMaster University. G. A. Botton is grateful to NSERC for the Discovery program funding.

## References

1. Z. Lu, D. D. MacNeil, and J. R. Dahn, *Electrochem. Solid-State Lett.*, **4**, A200 (2001).
2. D. D. MacNeil, Z. Lu, and J. R. Dahn, *J. Electrochem. Soc.*, **149**, A1332 (2002).
3. R. S. Arumugam, L. Ma, J. Li, X. Xia, J. M. Paulsen, and J. R. Dahn, *J. Electrochem. Soc.*, **163**, A2531 (2016).
4. J. Li, L. E. Downie, L. Ma, W. Qiu, and J. R. Dahn, *J. Electrochem. Soc.*, **162**, A1401 (2015).
5. J. A. Gilbert, I. A. Shkrob, and D. P. Abraham, *J. Electrochem. Soc.*, **164**, A389 (2017).
6. A. Jarry, S. Gottis, Y. S. Yu, J. Roque-Rosell, C. Kim, J. Cabana, J. Kerr, and R. Kostecki, *J. Am. Chem. Soc.*, **137**, 3533 (2015).
7. S. E. Sloop, J. B. Kerr, and K. Kinoshita, *J. Power Sources*, **119–121**, 330 (2003).
8. J. Self, C. P. Aiken, R. Petibon, and J. R. Dahn, *J. Electrochem. Soc.*, **162**, A796 (2015).
9. D. J. Xiong, R. Petibon, M. Nie, L. Ma, J. Xia, and J. R. Dahn, *J. Electrochem. Soc.*, **163**, 546 (2016).
10. J. C. Burns, A. Kassam, N. N. Sinha, L. E. Downie, L. Solnickova, B. M. Way, and J. R. Dahn, *J. Electrochem. Soc.*, **160**, A1451 (2013).
11. A. J. Smith, J. C. Burns, D. Xiong, and J. R. Dahn, *J. Electrochem. Soc.*, **158**, A1136 (2011).
12. X. Xia, J. Paulsen, J. Kim, and S.-Y. Han, *Lithium Nickel-Manganese-Cobalt Oxide Cathode Powders for High Voltage Lithium* Ion Batteries, (2016). Pat. No. WO2016116862A1
13. L. Zhu, J. Paulsen, H. S. AHN, and H. Hong, *Doped and Coated Lithium Transition Metal Oxide Cathode Materials for Batteries in Automotive Applications*, (2015). Pat. No. WO2015132647A1
14. L. Ma, J. Self, M. Nie, S. Glazier, D. Y. Wang, Y.-S. Lin, and J. R. Dahn, *J. Power Sources*, **299**, 130 (2015).
15. J. Xia, L. Ma, C. P. Aiken, K. J. Nelson, L. P. Chen, and J. R. Dahn, *J. Electrochem. Soc.*, **161**, A1634 (2014).
16. K. J. Nelson, J. Xia, and J. R. Dahn, *J. Electrochem. Soc.*, **161**, A1884 (2014).
17. J. Xia, N. N. Sinha, L. P. Chen, G. Y. Kim, D. J. Xiong, and J. R. Dahn, *J. Electrochem. Soc.*, **161**, A84 (2013).
18. D. Chen, W. Tu, M. Chen, P. Hong, X. Zhong, Y. Zhu, Q. Yu, and W. Li, *Electrochim. Acta*, **193**, 45 (2016).
19. H.-S. Kim, Y. Kim, S.-I. Kim, and S. W. Martin, *J. Power Sources*, **161**, 623 (2006).
20. Y. Kim, H. S. Kim, and S. W. Martin, *Electrochim. Acta*, **52**, 1316 (2006).
21. H. Liu, D. Qian, M. G. Verde, M. Zhang, L. Baggetto, K. An, Y. Chen, K. J. Carroll, D. Lau, M. Chi, G. M. Veith, and Y. S. Meng, *ACS Appl. Mater. Interfaces*, **7**, 19189 (2015).
22. S. Pang, Y. Wang, T. Chen, X. Shen, X. Xi, and D. Liao, *Ceram. Int.*, **42**, 5397 (2016).
23. Y.-K. Sun, M.-J. Lee, C. S. Yoon, J. Hassoun, K. Amine, and B. Scrosati, *Adv. Mater.*, **24**, 1192 (2012).
24. C. Wang and J. Zhang, *Chem. Mater.*, **26**, 6320 (2014).
25. J. Wang, C. Du, X. Xu, X. He, G. Yin, Y. Ma, P. Zuo, X. Cheng, and Y. Gao, *Electrochim. Acta*, **192**, 340 (2016).
26. P. Yan, J. Zheng, X. Zhang, R. Xu, K. Amine, J. Xiao, J.-G. Zhang, and C.-M. Wang, *Chem. Mater.*, **28**, 857 (2016).
27. Z. Zhu, F. Cai, and J. Yu, *J. Ionics*, **22** 1353 (2016).
28. J. Xia, Z. Lu, J. Camardese, and J. R. Dahn, *J. Power Sources*, **306**, 516 (2016).
29. K. J. Nelson, D. W. Abarbanel, J. Xia, Z. Lu, and J. R. Dahn, *J. Electrochem. Soc.*, **163**, A272 (2015).
30. J. R. Dahn and G. M. Ehrlich, in *Linden's Handbook of Batteries*, New York: McGraw-Hill (2011).
31. J. Jiang and J. R. Dahn, *Electrochim. Acta*, **49**, 2661 (2004).
32. L. Wang, B. Wu, D. Mu, X. Liu, Y. Peng, H. Xu, Q. Liu, L. Gai, and F. Wu, *J. Alloys Compd.*, **674**, 360 (2016).
33. S. Park, K. Chang, H.-K. Park, S. T. Hong, and Y. Choi, *Electrode Active Material for Lithium Secondary Battery*, (2014). Patnet No. US 20140356719 A1
34. H. Zhou, S. Zhang, X. Yang, and W. Wei, *Preparation Method of Lithium Ion Battery Ternary Cathode Material*, (2012). Patnet No. CN102509784A
35. M. Nie, J. Xia, and J. R. Dahn, *J. Electrochem. Soc.*, **162**, A1186 (2015).
36. A. Van Bommel and J. R. Dahn, *Chem. Mater.*, **21**, 1500 (2009).
37. J. Li, J. Camardese, S. Glazier, and J. R. Dahn, *Chem. Mater.*, **26**, 7059 (2014).
38. J. Li, J. Camardese, R. Shunmugasundaram, S. Glazier, Z. Lu, and J. R. Dahn, *Chem. Mater.*, **27**, 3366 (2015).
39. H. M. Dahn, a., J. Smith, J. C. Burns, D. a. Stevens, and J. R. Dahn, *J. Electrochem. Soc.*, **159**, A1405 (2012).
40. T. M. Bond, J. C. Burns, D. A. Stevens, H. M. Dahn, and J. R. Dahn, *J. Electrochem. Soc.*, **160**, A521 (2013).
41. C. P. Aiken, J. Xia, D. Y. Wang, D. a. Stevens, S. Trussler, and J. R. Dahn, *J. Electrochem. Soc.*, **161**, A1548 (2014).
42. L. J. Krause, L. D. Jensen, and J. R. Dahn, *J. Electrochem. Soc.*, **159**, A937 (2012).
43. Z. Lu, L. Y. Beaulieu, R. A. Donaberger, C. L. Thomas, and J. R. Dahn, *J. Electrochem. Soc.*, **149**, A778 (2002).
44. E. McCalla, G. H. Carey, and J. R. Dahn, *Solid State Ionics*, **219**, 11 (2012).
45. L. Ma, J. Xia, and J. R. Dahn, *J. Electrochem. Soc.*, **161**, A2250 (2014).
46. L. E. Downie and J. R. Dahn, *J. Electrochem. Soc.*, **161**, A1782 (2014).
47. S. L. Glazier, R. Petibon, J. Xia, and J. R. Dahn, *J. Electrochem. Soc.*, **164**, A567 (2017).
48. S. Bak, E. Hu, Y. Zhou, X. Yu, S. D. Senanayake, S. Cho, K. Kim, K. Y. Chung, X. Yang, and K. Nam, *ACS Appl. Mater. Interfaces*, **6**, 22594 (2014).
49. Q. Q. Liu, R. Petibon, C. Y. Du, and J. R. Dahn, *J. Electrochem. Soc.*, **164**, A1173 (2017).